Journal of Materials Science: Materials in Electronics (2020) 31:8844–8851
https://doi.org/10.1007/s10854-020-03419-2

Anodic oxidation growth of lanthanum/manganese-doped TiO_2 nanotube arrays for photocatalytic degradation of various organic dyes

Wenxuan Wang[1] · Jubo Zhang[1,2] · Daxin Liang[1,2,3] · Yudong Li[1,2] · Yanjun Xie[1,2] · Yonggui Wang[1,2] · Jian Li[1,2]

Received: 18 December 2019 / Accepted: 13 April 2020 / Published online: 22 April 2020

Abstract
Lanthanum/manganese-doped TiO_2 nanotube arrays (La/Mn-TNAs) can provide a greater catalytic area and possess stronger photocatalytic activity than TiO_2 nanotubes (Li et al. in Nano Res 8(3):900–906, (2015)). Due to the wide band gap, TiO_2′s capacity to capture visible light is low, and TiO_2 (3.2 eV) can only absorb ultraviolet light. To resolve this issue, most researchers doped TiO_2 with nitrogen. In this paper, we doped transition metal ions and rare earth metal ions in TiO_2 nanotube arrays to decrease their band gaps, improving the activities of photocatalysts. In addition, La/Mn-TNAs were obtained by anodizing a Ti foil in the electrolyte. Additionally, the photocatalytic activity of the sample was evaluated by analyzing the degradation rate of organic pollutants. As a result, when the Ti foil was anodic oxidation for 3 h and contained 4.8 wt% of lanthanum and manganese, it could degrade organic dyes entirely in 60 min and the degradation rate of organic dyes was over 95%. Thus, La/Mn-TNAs can satisfy people's requirement of rapid degradation of organic pollutants.

1 Introduction

Nowadays, environment pollution is the most typical issue caused. Addressing the environment pollution is crucial. Along with the discovery of advanced oxidation processes (AOPs) [1, 2], a large number of photocatalytic materials have been discovered and applied to life. As metal oxides photocatalysts and semiconductive photocatalysts, ZnO [3], WO_3 [4], CdS [5], ZnS [6], SnO_2 [7] and Fe_3O_4 [8], are difficult to recover in the reaction system, the environment is subject to secondary pollution. By contrast, TiO_2 nanotube array is a photocatalysis with a relatively large volume in the macro, which fundamentally circumvents this problem. And TiO_2 nanotube arrays is low operational and installation cost. So TiO_2 is widely used as photocatalysts owing to its properties including unique structure, greater catalytic area, better adsorption ability and favorable degradation requirements with low carbon emission and a friendly environment in recent years [9]. So TiO_2 becomes the catalyst for photocatalytic oxidation [10], which produces many reactive hydroxyl radicals in the solution as the intermediate product of the reaction, which can respond directly to the pollutants in the wastewater. Besides, TiO_2 is a kind of n-type semiconductor with good photocatalytic performance [11]. It can make full use of solar energy to degrade organic pollutants, which is an efficient and environmentally friendly process [12]. However, it is well known that TiO_2 has a wide band gap (3.2 eV) [13] and a high recombination rate of photogenerated electron–hole pairs; unfortunately, these two shortcomings haven't been overcome completely [14]. Fortunately, metal ion doping [15], non-metal ion doping [16, 17], co-doping [18], and semiconductor doping

Wenxuan Wang and Jubo Zhang have contributed equally to this work.

Electronic supplementary material The online version of this article (https://doi.org/10.1007/s10854-020-03419-2) contains supplementary material, which is available to authorized users.

✉ Daxin Liang
daxin.liang@nefu.edu.cn

✉ Yanjun Xie
yxie@nefu.edu.cn

[1] College of Materials Science and Engineering, Northeast Forestry University, Harbin 150040, People's Republic of China

[2] Key Laboratory of Bio-Based Material Science and Technology, Ministry of Education, Northeast Forestry University, Harbin 150040, China

[3] State Key Laboratory of Bio-Fibers and Eco-Textiles, Qingdao University, Qingdao 266071, Shandong, China

[19] can improve the photocatalytic capacity of TiO_2 by narrowing the band gap of TiO_2. We have obtained La/Mn-TNAs prepared by anodic oxidation. Lanthanum ion (La^{3+}), which is a less oxidized than titanium ion (Ti^{4+})[20], and the radius of La^{3+} (1.06 Å) is much larger than Ti^{4+} (0.53 Å), which will cause lattice distortion and expansion of TiO_2. Both can inhibit photo-generated electron–hole pair coupling [21]. And the radius of Mn^{3+} (0.58 Å) is smaller than Ti^{3+} (0.67 Å), it can replace the titanium dioxide lattice easily [22], and an intermediate energy level will be generated at 0.69 eV within the valence band of TiO_2, which make the valence electrons excited to jump from the middle doped level to the conduction band; this can greatly reduce the width of the forbidden band (shown in Fig S1). At the same time, the manganese of various valence states can increase the chance of doping success and obtain multiple doping levels [23], which is more conducive to broadening the range of the optical response of titanium dioxide.

When energy of irradiation on the TiO_2 nanotubes, the energy is greater than its forbidden gap. Its valence band generates electrons (e^-) that will be transferred to the conduction band and at the same time, generates holes (h^+) in valance band with hydroxyl radicals (HO•) generation from hydrogen peroxide(H_2O_2) by reacting with electrons (e^-)[24]. The mechanism of photochemical catalysis is as follows (also shown in Fig. 1):

In this study, we have recently obtained La/Mn-TNAs prepared by anodic oxidation. It is speculated that the morphology of La/Mn-TNAs, annealing temperature, and annealing time were determined by the efficiency of the electron–hole recombination process. Additionally, the formation efficiency of hydroxyl radicals was evaluated from the degradation efficiency under ultraviolet and visible light irradiation.

2 Experiment

2.1 Materials

A titanium plate was purchased from Dongcheng Lilin Metal Materials Business Department of Dongguan. Lanthanum nitrate ($La(NO_3)_3$), potassium permanganate ($KMnO_4$), ammonium fluoride (NH_4F), sodium sulfite (Na_2SO_3), silver nitrate ($AgNO_3$), 5,5-dimethyl-1-pyrroline N-oxide (DMPO), acetone, glycerol, hydrogen peroxide (30%), ethanol, xylenol orange (XO), rhodamine B (RhB), and methylene blue (MB) were purchased from Tianjin Kemiou Chemical Reagent Co., Ltd. (Tianjin, China). All the chemicals were of analytical reagent grade and could thus be used without further purification.

2.2 Synthesis of La/Mn-TNAs

Before anodization, the Ti plates were ultrasonically treated in acetone for 20 min and ethanol for 10 min and dried in a nitrogen stream. The anodization was carried out by using a two-electrode system with a Ti plate as the anode and Pt plate as the cathode. The distance between the electrodes was 4 cm. All anodization processes were carried out at room temperature. The anodization took place in the electrolyte composed of 50 mL glycerol, 50 mL H_2O, 0.6077 g NH_4F, 0.1244 g $La(NO_3)_3$ and 0.1244 g $KMnO_4$. The Ti plate reacted for 60–300 min at the applied voltage 25 V by using DC power supply. Finally, the obtained samples were washed with deionized water, dried in nitrogen and annealed for 5 h or 6 h at the temperature of 500 °C (heating rate: 3 °C/min). The experimental device and the flowchart are illustrated in Fig. 2. Simultaneously, the samples under different reaction conditions were presented in Table 1.

$$TiO_2 \rightarrow h^+ + e^- \quad (1)$$

$$H_2O_2 + e^- \rightarrow 2HO\bullet \quad (2)$$

$$H_2O_2 + HO\bullet \rightarrow \bullet OH_2 + H_2O \quad (3)$$

$$RH + HO\bullet \rightarrow R\bullet + H_2O \quad (4)$$

$$R\bullet + O_2 \rightarrow RO_2\bullet \quad (5)$$

$$RO_2\bullet + H_2O \rightarrow \text{Further reaction} \quad (6)$$

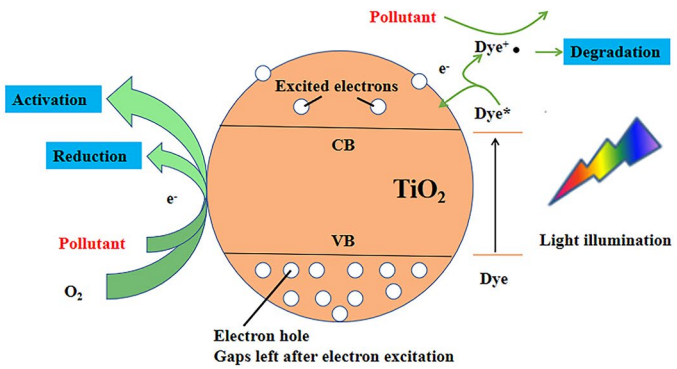

Fig. 1 Proposed mechanism of dye degradation under light illumination using TiO_2 nanotube arrays photocatalysis

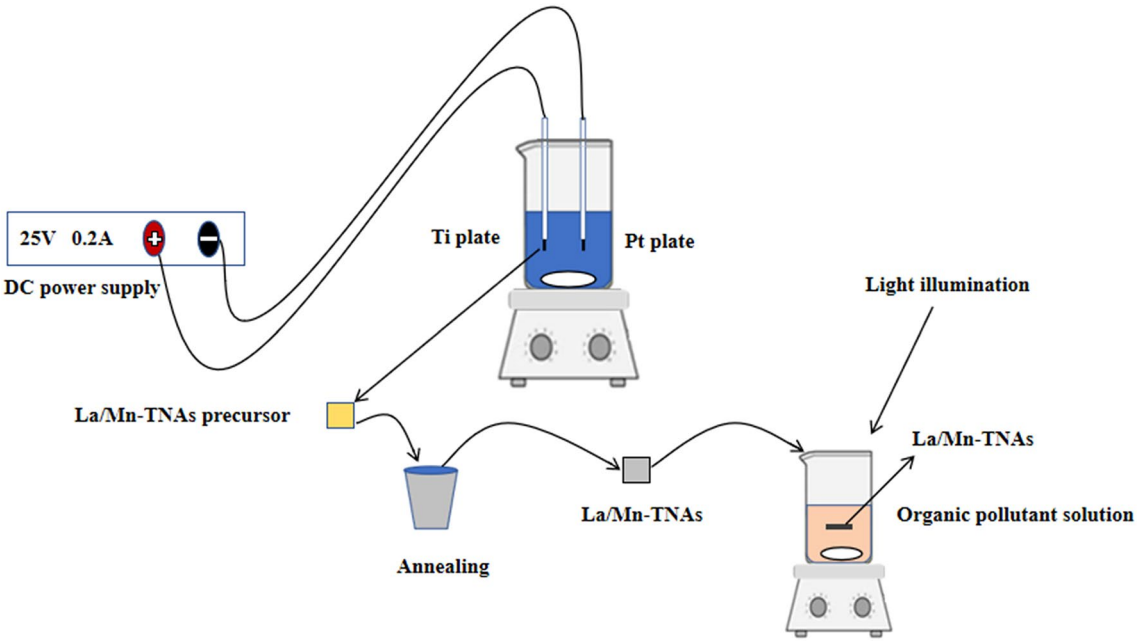

Fig. 2 The device and flowchart of synthesis of La/Mn-TNAs

Table 1 Sample number under different reaction conditions

Sample number	Oxidation time (h)	Annealing temperature (°C)	Annealing time (h)
1-500-5	1	500	5
2-500-5	2	500	5
3-500-5	3	500	5
4-500-5	4	500	5
5-500-5	5	500	5
3-500-6	3	500	6
3-550-5	3	550	5
3-550-6	3	550	6
3-600-5	3	600	5
3-600-6	3	600	6

2.3 Photocatalytic activity measurements

The photocatalytic activities of the as-synthesized La/Mn-TNAs were evaluated using a photocatalytic reactor equipped with a tubular mercury lamp (125 W) and xenon lamp (125 W). First, La/Mn-TNAs sheet (the area is 2*0.2*0.2 cm^2) was added to 40 mL of an organic dye (XO or RHB or MB) aqueous solution (20 mg/L), and 15 mL of H_2O_2 (30%) was then added to the reactor. Before being illuminated by UV or visible light, the reaction was ultrasonically mixed for 30 min to ensure a fine mixture of the photocatalyst and the solution and the equilibration of adsorption and desorption of organic dyes on the nanotube arrays. Finally, over a time of 60 min, the reacting solution was collected every 10 min.

2.4 Optimization of experimental conditions

The influencing factors of the photocatalytic activity during the degradation of organic dyes were evaluated by the initial ratio of reactants, the amount of H_2O_2 (30%) added and the pH of the reaction system.

2.5 Characterization

In this study, the crystal structure of the synthesized titanium dioxide nanotubes was determined by X-ray diffraction (XRD) using an X-ray diffractometer, which was Rigaku D/max and 2200 V/PC (copper Kα, $\lambda = 0.15418$ nm). Besides, on the basis of scanning electron microscopy (SEM) and an energy dispersive X-ray analysis system (EDS), the researcher mapped the sample, characterized it, and analyzed the element by JSM-7500F scanning electron microscopy in this experiment. X-ray photoelectron spectra (XPS) were conducted on a VGESCALAB250 spectrometer. Diffuse reflectance spectra were recorded using a double-beam thermostat spectrometer Cary 100-Varian. Through the specific surface area test, the catalytic area was obtained, and the JW-BK132F microporous analyzer was used for the test. Then, the degradation of XO, RhB and MO was evaluated by a Beijing Puxi TU-1901 UV–Visible spectrophotometer.

3 Results and discussion

3.1 XRD analysis

Figure 3a shows the various situations of oxidation of the titanium sheet from 1 to 5 h when annealing temperature at 500 °C. The characteristic peaks of anatase appeared at 25.325°, 37.841°, and 48.074° when the crystal faces of tetragonal TiO_2 (anatase phase) reflected to (101), (004), and (200), respectively. These peaks are consistent with the reference data set (JCPDS NO. 71–1166). In addition, in Fig. 3a, no peaks of impurities are presented; this indicated the high purity of the sample.

Figure 3b illustrates the XRD test of titanium dioxide nanotube arrays at different annealing temperatures. When the samples were annealed at 500 °C, the sharper the diffraction peak, the higher the crystallinity of anatase. Above 550 °C, the anatase (101) characteristic peak gradually weakened; the rutile (110) phase gradually increased; and anatase was further converted into rutile. To sum up, the optimum oxidation time of the titanium dioxide nanotube arrays was 3 h, and the optimum annealing temperature was 500 °C.

3.2 Elemental analysis

Energy dispersive spectroscopy (EDS) was used to detect the elemental of the as-synthesized sample. Figure 4a and b clearly illustrates the presence of Ti, O, La, and Mn on the surface and inside of the sample. X-ray photoelectron spectroscopy (XPS) was used to analysis the contents of various elements, which was shown in Fig. S2. By integrating the peak areas under the XPS peaks of the dopants, an estimate of the amount of doping can be obtained, and the contents of various elements was shown in Table S1. This presence is consistent with the element ratio of reactants, suggesting that La and Mn were successfully doped in the TiO_2 nanotube arrays.

3.3 SEM analysis

Figure 5 presents the TiO_2 nanotube arrays with highly ordered surfaces, in which the nanotube diameter is 80–100 nm (a) and nanotube length is approximately 1.5–2 μm (b). The diameters of the anodic oxidation of TiO_2 nanotube arrays were between 80 and 100 nm in 1, 2, and 3 h, respectively, when the corresponding lengths of the TiO_2 nanotube arrays were 110, 160, and 195 μm. However, when the oxidation time was 4 h or longer, the length of the nanotube arrays was lowered and the nanotube arrays collapsed. The titanium dioxide matrix was reconstituted when the oxidation time was 5 h. Therefore, the main role of the anodization time was to lengthen the TiO_2 nanotube arrays to obtain longer TiO_2 nanotube arrays. In particular, oxidation time could bring about the collapse and reconstruction of the matrix and the continuous growth of the nanotubes.

3.4 Specific surface area analysis

Specific surface areas were examined using the Brunauer–Emmett–Teller (BET) method. The BET test indicated that the specific surface area of the TiO_2 nanotube arrays reached 26.44339 (m^2/g), which greatly increased the specific surface area of the titanium foil. At the same time, the contact area with the solution was greatly increased, so that the rate of catalytic degradation is greatly improved.

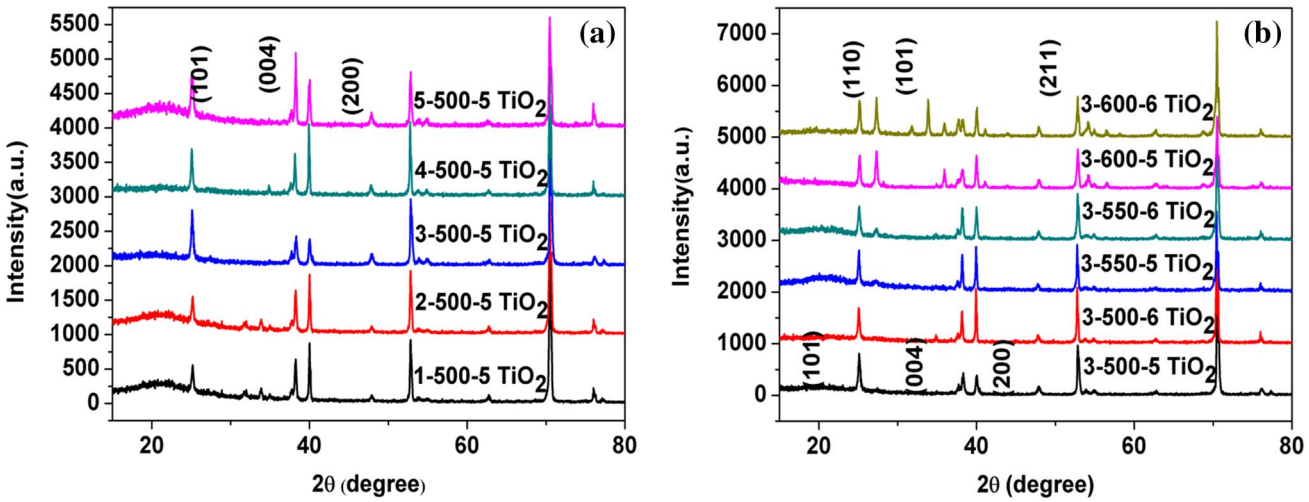

Fig. 3 XRD patterns of La/Mn-TNAs

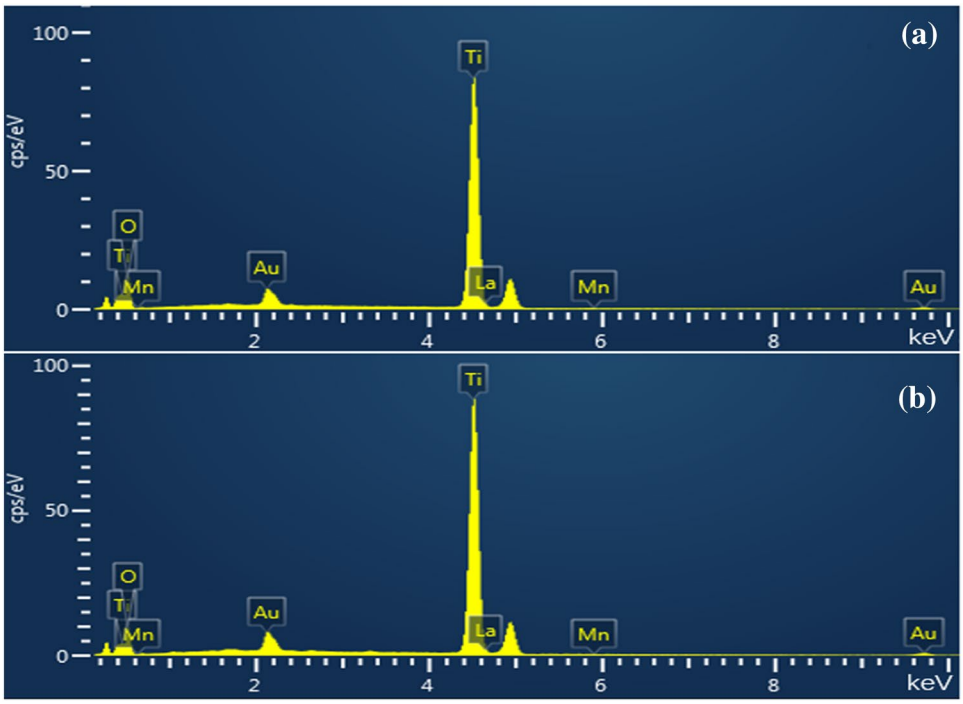

Fig. 4 EDS of La/Mn-TNAs, **a** sample surface and **b** cross-section of sample

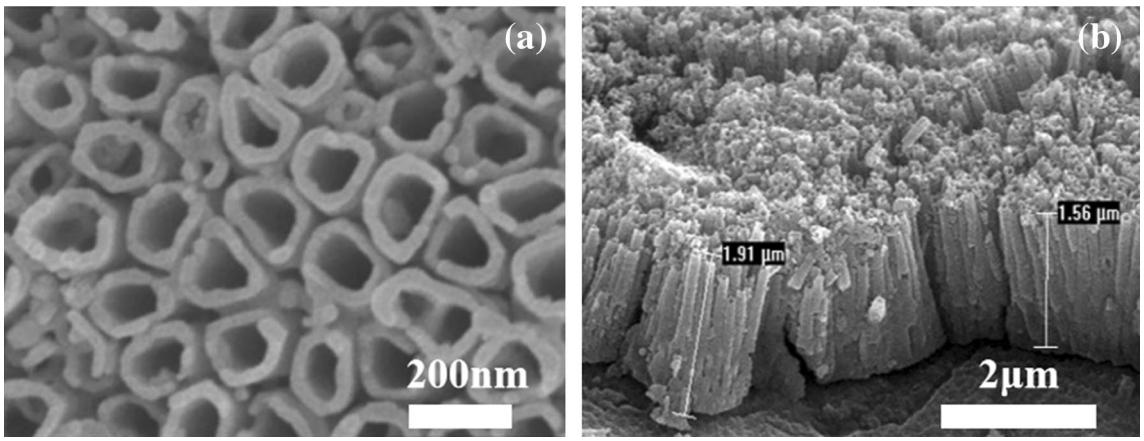

Fig. 5 SEM images of La/Mn-TNAs, **a** sample surface at 5.0KV and **b** cross-section of sample at 20.0KV

3.5 Photocatalytic degradation properties

The degradation processes of organic dyes by samples prepared in different reaction conditions were studied under UV light (high-pressure mercury lamp, 375 W, 200–400 nm) and visible light (high-pressure xenon lamp, 375 W, 400–800 nm). The doping of La and Mn to TiO_2 nanotube arrays reduces the band gap of it from 3.09 eV (Fig. S1(a)) to 2.76 eV (Fig. S1(b)), allowing the holes and electrons in La/Mn-TNAs to be excited from the valence band to the conduction band by visible light, and the photocatalytic efficiency is considerably enhanced compared with pure TiO_2 nanotube arrays (Fig. S3). As presented in Table 2, 10 different samples indicated the degradation rate of RhB, XO, and MB all above 50% in 10 min. As illustrated in Fig. 6 and Table 2, it is clear that the degradation rates of RhB, MB, and XO reach 69.47%, 76.44%, and 80.41%, respectively, when the photocatalytic reaction time reaches 10 min. The degradation rates of RhB, MB, and XO, respectively, reach 99.47%, 96.44%, and 99.31% when the photocatalytic reaction time reaches 60 min.

3.6 Radical scavenger study

Radical scavenger study was used for obtain insights to the photocatalytic reaction mechanism in La/ Mn-TNAs. The

Table 2 Degradation rate of different samples in 10 min

Sample number	Degradation rate of RhB in 10 min (%)	Degradation rate of MB in 10 min (%)	Degradation rate of XO in 10 min (%)
1-500-5	51.08	64.60	54.35
2-500-5	66.53	58.81	53.41
3-500-5	66.47	66.41	71.29
4-500-5	43.47	59.55	63.32
5-500-5	68.47	72.1	56.02
3-500-6	69.47	76.44	80.41
3-550-5	52.90	71.13	56.47
3-550-6	66.47	71.06	67.52
3-600-5	67.69	67.69	73.64
3-600-6	63.72	63.72	61.41

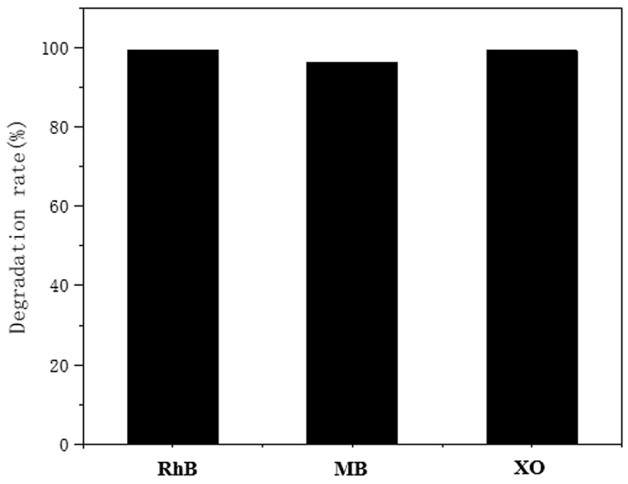

Fig. 6 Degradation rate of RhB, MB, and XO using the as-synthesized TiO_2 nanotube arrays under UV light

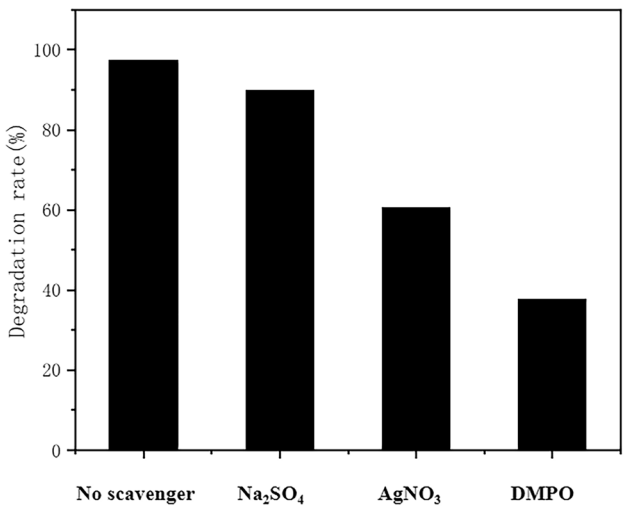

Fig.7 RhB degradation rates with radical scavengers

same wight Na_2SO_4, $AgNO_3$, and DMPO were added to the reactor as hole scavenger, electron scavenger, and radical scavenger before being illuminated. UV–Vis spectra of RhB dyes with degradation were shown in Fig. S4. The degradation rates of RhB in 50 min with no scavenger, Na_2SO_4, $AgNO_3$, and DMPO were 97.43, 89.77%, 60.51%, and 37.60% (Fig. 7). These results can demonstrate the photocatalytic reaction mechanism of La/Mn-TNAs.

3.7 Influence of pH on photocatalytic degradation of XO, RhB, and MB

HCl and NaOH were utilized to adjust pH values of organic dye (XO, RhB, and MB) solutions in the range of 1–13 to determine the influence of pH on the degradation behavior. As illustrated in Fig. 8, in acidic and neutral conditions, when photocatalytic reaction time reaches 40 min, the degradation rates of organic dyes (RhB, MB, and XO) all came close to 100%. Additionally, in alkaline conditions, when photocatalytic reaction time reaches 40 min, the degradation rates of organic dyes (RhB, MB, and XO) are less than 85%, and the degradation rate of the photocatalytic reaction is only 90% when photocatalytic reaction reaches 60 min. The degradation rate curve can be found in which the degradation effect of acidic and neutral conditions is better than that of alkaline conditions.

4 Conclusions

In this work, La/Mn-TNAs with nanotube diameters of 80–100 nm and lengths of approximately 1.5–2 μm were successfully synthesized using the anodic oxidation method. The as-synthesized La/Mn-TNAs had excellent photocatalytic performance for the degradation of organic dyes (XO, RhB, and MB) and with degradation rates above 90%. The doping of La and Mn to TiO_2 nanotube arrays has significant effect on the absorption properties of TiO_2 and effectively

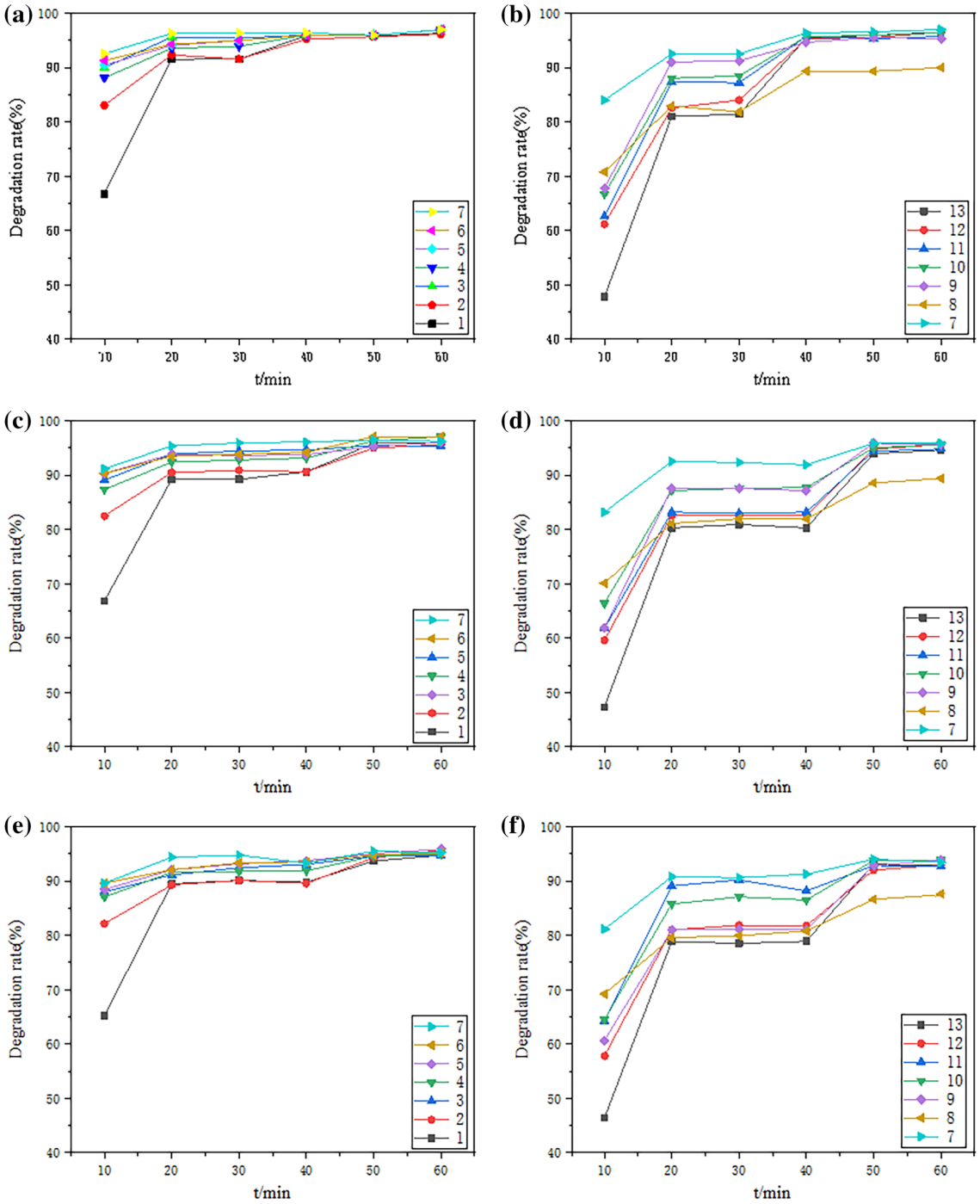

Fig. 8 UV–Vis spectra of organic dyes with degradation at different pH values by various substances. **a**, **b** rhodamine B; **c**, **d** methylene blue; and **e**, **f** xylenol orange

narrows the band gap, which can promote its photocatalytic activity. After intensive investigation, efficient photocatalytic property can be obtained when pH ranges from 1 to 13, and the highest degradation rate emerged when the initial mass ratio of the reactants for 3 h of annealing at 550 °C for 5 h at pH 7. Thus, the as-synthesized La/Mn-TNAs could be promising candidates for the practical degradation of organic dyes in waste water.

Acknowledgements This work was supported by the Fundamental Research Funds for the Central Universities (2572018BB05), the Natural Science Foundation of Heilongjiang Province (YQ2019C004), and the State Key Laboratory of Bio-Fibers and Eco-Textiles (2017kfkt06).

We thank LetPub (www.letpub.com) for its linguistic assistance during the preparation of this manuscript.

Compliance with ethical standards

Conflict of interest The authors report no conflicts of interest.

References

1. H. Li, Q. Zhou, Y. Gao, X. Gui, L. Yang, M. Du, E. Shi, J. Shi, A. Cao, Y. Fang, Nano Res. **8**(3), 900–906 (2015)
2. S. Esplugas, J. Giménez, S. Contreras, E. Pascual, M. Rodríguez, Water Res. **36**, 1034 (2002)
3. F. Lu, W. Cai, Y. Zhang, Adv. Funct. Mater. **18**, 1047 (2010)
4. J.Z. Ou, S. Balendhran, M.R. Field, D.G. Mcculloch, A.S. Zoolfakar, R.A. Rani, S. Zhuiykov, A.P. O'Mullane, K. Kalantar-Zadeh, Nanoscale **4**, 5980 (2012)
5. D.J. And, L. Guo, J. Phys. Chem. B **110**, 11139 (2006)
6. H.C. Swart, L. Oosthuizen, P.H. Holloway, G.L.P. Berning, Surf. Interface Anal. **26**, 337 (2015)
7. L. Zheng, Y. Zheng, C. Chen, Y. Zhan, X. Lin, Q. Zheng, K. Wei, J. Zhu, Inorg. Chem. **48**, 1819 (2009)
8. K. Zheng, M. Di, J. Zhang, W. Bao, D. Liang, G. Pang, Z. Fang, C. Li, Chem. Res. Chin. Univ. **33**, 1 (2017)
9. M.B. Ray, J.P. Chen, L.K. Wang, S.O. Pehkonen, Treatise on Water Sci. **4**, 377 (2006)
10. S. Sato, R. Nakamura, S. Abe, Appl. Catal. A **284**, 131 (2015)
11. Y. Zhang, Z.R. Tang, X. Fu, Y.J. Xu, ACS Nano **4**, 7303 (2014)
12. X. He, Y. Cai, H. Zhang, C. Liang, Phys. Rev. Lett. **104**, 036806 (2010)
13. L. Wan, J.F. Li, J.Y. Feng, W. Sun, Z.Q. Mao, Mater. Sci. Eng. B-Adv. **139**, 216 (2007)
14. Z. Frontistis, C. Drosou, K. Tyrovola, D. Mantzavinos, D. Fattakassinos, D. Venieri, N.P. Xekoukoulotakis, Ind. Eng. Chem. Res. **51**, 16552 (2017)
15. J. Xiao, C. Wang, S. Lyu, H. Liu, J.C. Jiang, Y. Lei, Sep. Purif. Technol. **169**, 202 (2016)
16. L.G. Devi, R. Kavitha, Appl. Catal. B **140–141**, 559 (2013)
17. K. Shankar, K. Chhay Tep, G.K. Mor, C.A. Grimes, J. Phys. D **39**, 2361–2366 (2006)
18. Z. Yu, L. Yang, C. Sheng, X. Wang, Y. Ma, W. Qiang, Z. Hu, J. Am. Chem. Soc. **135**, 1201 (2013)
19. G. Pliego, J.A. Zazo, P. Garciamuñoz, M. Munoz, J.A. Casas, J.J. Rodriguez, Desalin. Water Treat. **57**, 9837 (2015)
20. F. Torrades, J. García-Montaño, Dyes Pigm. **100**, 184 (2014)
21. A. Mohammadpour, P. Kar, B.D. Wiltshire, A.M. Askar, K. Shankar, Current Nanoscience (2015). https://doi.org/10.2174/1573413711666150415230019
22. G.C. Silva, F.S. Almeida, A.M. Ferreira, Mater. Res. **15**, 403 (2012)
23. W. Wei, X. Cui, W. Chen, D.G. Ivey, Chem. Soc. Rev. **40**, 1697 (2011)
24. J. Yu, G. Dai, B. Huang, J. Phys. Chem. C **113**, 16394 (2009)